J. Fluid Mech. (1983), *vol.* 135, *pp.* 389–405
Printed in Great Britain

Computer extension and analytic continuation of Blasius' expansion for impulsive flow past a circular cylinder

By S. J. COWLEY†

Department of Applied Mathematics and Theoretical Physics, University of Cambridge, Silver Street, Cambridge CB3 9EW

(Received 2 May 1983)

Boundary-layer flow past an impulsively started cylinder is studied by extending the Blasius time-series expansion to many terms. The ordinary differential equations that result from this expansion are solved using an $O(h^6)$-accurate numerical method. The validity of the simple series expansions for the wall shear, displacement thickness and viscous displacement velocity is extended by recasting the series using rational functions. The solutions so obtained are in good agreement with previous authors' work. In particular, an examination of the poles and zeros of the rational functions confirms that a singularity develops within a finite time. The analytic structure of the singularity is found to be in agreement with the asymptotic expansion proposed by van Dommelen & Shen.

1. Introduction

An important question in unsteady large-Reynolds-number flow is how an initially attached boundary-layer solution develops into a separated flow including detached free shear layers. An often-studied model problem is that of a circular cylinder of infinite length which suddenly starts to move through a viscous incompressible fluid in a direction at right angles to its axis (figure 1). Experiments illustrating the development of this flow have been performed by Nagata, Minami & Murata (1979) and Bouard & Coutanceau (1980).

Previous theoretical work on this problem can be split into two main categories. The first consists of numerical solutions of the Navier–Stokes equations at finite Reynolds numbers R. Solutions for $R \gtrsim 200$ have been found by, *inter alia*, Thoman & Szewczyk (1969), Son & Hanratty (1969), Dennis & Staniforth (1971), Collins & Dennis (1973*a*), Patel (1976) and Ta Phuoc Loc (1980). Solutions of the second category are those for which the boundary-layer approximation has been used. The first of these was obtained by Blasius (1908), who sought a series solution in powers of time. He obtained the first two terms of the series, and was able to calculate a first approximation to the time at which the flow reverses at the rear of the cylinder. Further terms of the series were calculated by Goldstein & Rosenhead (1936), Wundt (1955) and Collins & Dennis (1973*b*). This series method of solution has also been extended to finite but large Reynolds numbers, by Wang (1967), Collins & Dennis (1973*b*) and Bar-Lev & Yang (1975).

Finite-difference solutions of the boundary-layer equations using an Eulerian

† Present address: Department of Mathematics, University College London, London WC1E 6BT.

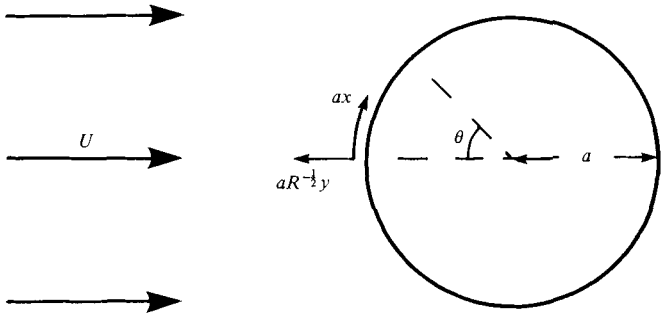

FIGURE 1. Flow past a circular cylinder. x and θ are measured in radians and degrees respectively.

coordinate system have been obtained by Dennis & Staniforth (1971), Collins & Dennis (1973*a*), Cebeci (1979, 1982) and Wang (1979, 1982). Van Dommelen & Shen (1980) have also presented a finite-difference solution. In a novel approach, they used a Lagrangian coordinate system, and found that a singularity develops in the unsteady boundary-layer equations after a finite time. The numerical solution of Ingham (1983), based on a series-truncation method, also supports the existence of this singularity. The aim of this paper is to solve the classical boundary-layer equations by numerically extending the series solution of Blasius (1908) to many terms. Flow quantities of interest are obtained by recasting the series using rational functions. Good agreement is found with previous results. Further, from a study of the positions of the poles and zeros of the rational functions, it is possible to obtain insight into the analytical structure of the solution. In particular, an examination of the viscous displacement velocity confirms the existence of a singularity.

2. Mathematical formulation

The unsteady boundary-layer equation and boundary conditions describing incompressible flow past an impulsively started circular cylinder, as given by, for example, Batchelor (1967) or Schlichting (1968) are

$$\psi_{yt}+\psi_y\psi_{yx}-\psi_x\psi_{yy}=\sin x\cos x+\psi_{yyy}, \tag{2.1a}$$

$$\psi=0 \quad \text{for} \quad t<0, \tag{2.1b}$$

$$\psi=0, \quad \psi_y=0 \quad \text{on} \quad y=0, \tag{2.1c}$$

$$\psi_y\to\sin x \quad \text{as} \quad y\to\infty, \quad t\geqslant 0. \tag{2.1d}$$

The Cartesian coordinate x is measured along the surface of the cylinder from the front stagnation point,† while y is measured from the cylinder surface along the local normal (see figure 1). ψ is the stream function and t is the time coordinate. The variables x, y, t and ψ have been non-dimensionalized by a, $aR^{-\frac{1}{2}}$, $a/2U$ and $2UaR^{-\frac{1}{2}}$ respectively, where a is the radius of the cylinder, U is the velocity of the cylinder, and $R=2Ua/\nu$ is the Reynolds number of the flow for a fluid with viscosity ν. Following Blasius (1908), the impulsive start is accounted for by the transformation

$$\eta=\frac{y}{2t^{\frac{1}{2}}}, \quad \psi=2t^{\frac{1}{2}}\phi(x,\eta,t), \tag{2.2a}$$

† x is measured in radians. The equivalent angle in degrees will be referred to by θ.

and ϕ is expanded as a power series in time:

$$\phi = \sum_{r=0}^{\infty} \phi_r(x, \eta)\, t^r. \tag{2.2b}$$

Since the pressure gradient is a simple sinusoidal function, the $\phi_r(x, \eta)$ can be further expanded as

$$\phi_r = \sum_{p=1}^{r+1} \sin px f_{rp}(\eta). \tag{2.2c}$$

On substituting (2.2) into (2.1*a*), rearranging the nonlinear terms, and equating the coefficients of each of the $t^r \sin px$ terms, it is found that if $r+p$ is even then $f_{rp} \equiv 0$, and that if $r+p$ is odd then

$$f'''_{rp} + 2\eta f''_{rp} - 4r f'_{rp} = 2(S_{1rp} + S_{2rp} - S_{3rp} - \delta_{1r}). \tag{2.3a}$$

The double sums S_{jrp} are given by

$$S_{1rp} = \sum_{j=0}^{r-1} \sum_{n=\max(1,\, p+j-r)}^{\min(j+1,\, p-1)} n(f'_{jn} f'_{k\,p-n} - f_{jn} f''_{k\,p-n}), \tag{2.3b}$$

$$S_{2rp} = \sum_{j=0}^{r-1-p} \sum_{n=1}^{\min(j+1,\, r-j-p)} n(f'_{jn} f'_{k\,p+n} - f_{jn} f''_{k\,p+n}), \tag{2.3c}$$

$$S_{3rp} = \sum_{j=p}^{r-1} \sum_{n=p+1}^{\min(j+1,\, r-j+p)} n(f'_{jn} f'_{k\,n-p} - f_{jn} f''_{k\,n-p}), \tag{2.3d}$$

where $k = r-1-j$, and the sums are zero if the upper bound of the index is less than the lower bound. Here a prime denotes differentiation with respect to η. The accompanying boundary conditions, deduced from (2.1*b–d*), are

$$f_{rp}(0) = f'_{rp}(0) = 0 \quad \text{for} \quad r \geqslant 0, \quad 1 \leqslant p \leqslant r+1, \tag{2.4a}$$

$$f'_{01} \to 1, \quad f'_{rp} \to 0 \quad \text{as} \quad \eta \to \infty, \quad r \geqslant 1, \quad 1 \leqslant p \leqslant r+1. \tag{2.4b}$$

Blasius (1908) and Goldstein & Rosenhead (1936) have found analytical solutions for $r \leqslant 2$ in terms of exponential and error functions. However, analytical solutions for the higher-order terms rapidly become unwieldy. It was therefore decided to solve (2.3) numerically.

3. Numerical solution

Following Collins & Dennis (1973*b*), the system of equations (2.3) was solved using an $O(h^4)$-accurate finite-difference scheme. This scheme, described by Fox (1957), works for second-order equations involving no first derivatives. Hence the transformations $f'_{rp} = e^{-\frac{1}{2}\eta^2} H_{rp}$ and $f''_{rp} = e^{-\frac{1}{2}\eta^2} \Omega_{rp}$ were introduced. The governing equations (2.3a) then become

$$H''_{rp} - (4r+1+\eta^2) H_{rp} = 2e^{\frac{1}{2}\eta^2} (S_{1rp} + S_{2rp} - S_{3rp} - \delta_{1r}), \tag{3.1a}$$

$$\Omega''_{rp} - (4r-1+\eta^2) \Omega_{rp} = 2e^{\frac{1}{2}\eta^2} (S'_{1rp} + S'_{2rp} - S'_{3rp}). \tag{3.1b}$$

Denoting values at three successive grid points of a uniform grid of size h by the subscripts $j-1$, j and $j+1$, the finite-difference approximation to (3.1*a*) used was

$$(1 - \tfrac{1}{12}\alpha_{j-1} h^2)(H_{rp})_{j-1} - (2 + \tfrac{5}{6}\alpha_j h^2)(H_{rp})_j + (1 - \tfrac{1}{12}\alpha_{j+1} h^2)(H_{rp})_{j+1}$$
$$= \tfrac{1}{12} h^2 (\beta_{j+1} + 10\beta_j + \beta_{j+1}), \tag{3.2}$$

where $\alpha(\eta) = 4r + 1 + \eta^2$, and $\beta(\eta)$ is the right-hand side of (3.1*a*). Similar finite-difference formulae can be found (i) for the Ω_{rp} from (3.1*b*), and (ii) for the f_{rp} in terms of Ω_{rp}.

The boundary conditions to apply to H_{rp} and f_{rp} on $\eta = 0$ follow directly from (2.4*a*), while the boundary conditions valid as $\eta \to \infty$ were replaced by asymptotic conditions imposed on $\eta = \eta_\infty$. For instance, $H_{rp} \sim \lambda \eta^{-q} e^{-\frac{1}{2}\eta^2}$ as $\eta \to \infty$, where λ and q are constants. Hence $H'_{rp}(\eta_\infty) \sim -\eta_\infty H_{rp}(\eta_\infty)$. The use of asymptotic conditions instead of $H'_{rp}(\eta_\infty) \approx 0$ proved to be a necessary improvement on previous authors' work. The outer boundary conditions on the Ω_{rp} were also replaced by asymptotic boundary conditions. However, there is no straightforward boundary condition to apply to the Ω_{rp} on $\eta = 0$. The following procedure was therefore adopted. First, (3.1*b*) was integrated to find the particular solution $\tilde{\Omega}_{rp}$ with $\tilde{\Omega}_{rp}(0) = 0$, then the complementary function $\hat{\Omega}_{rp}$ of (3.1*b*) satisfying $\hat{\Omega}_{rp}(0) = 1$ was found. Using Romberg's method, $\tilde{f}'_{rp}(0)$ and $\hat{f}'_{rp}(0)$ were next calculated by integrating $e^{-\frac{1}{2}\eta^2}\tilde{\Omega}_{rp}$ and $e^{-\frac{1}{2}\eta^2}\hat{\Omega}_{rp}$ respectively from 0 to ∞. Finally, the necessary multiple of the complementary function was added to the particular solution in order to yield $f'_{rp}(0) = 0$.

The tridiagonal matrices resulting from the finite-difference approximation were solved by Gaussian elimination with partial pivoting. In addition, two step sizes h and $2h$ were used so that the solutions could be extrapolated to give $O(h^6)$ accuracy.

The calculations were performed on an IBM 3081. In order to check round-off error, runs were made in both double- and quadruple-precision arithmetic (16 and 33 figures respectively). The accuracy of the final solution was checked by varying both the number of grid points N and position of the outer boundary η_∞ (note that $h = \eta_\infty/N$).

Comparisons were made between the present finite-difference solutions and the exact solutions for the first three terms found by Blasius (1908) and Wundt (1955). Good agreement was found, and the $O(h^6)$ accuracy of our method was confirmed. The present results also agreed with the finite-difference solutions for the first eight terms found by Collins & Dennis (1973*b*).

A comparison of runs with $\eta_\infty = 14$, $N = 768$ and $\eta_\infty = 15$, $N = 1200$ suggests that, for $r = 46$, $\max_p |f''_{rp}(0)|$ and $\max_p |f_{rp}(\infty)|$ are known to at least 3 and 7 significant figures respectively. The numerical values of the f_{rp} etc. are not tabulated here, but are available from the author on request. The data from a quadruple-precision run with $\eta_\infty = 15$ and $N = 1200$ have been used to produce the results in the rest of this paper. This run, which calculated 51 terms of the series (i.e. the maximum value of r is 50), required $4\frac{1}{2}$ h of CPU time. The long run time is a result of both the slowness of quadruple-precision arithmetic and the $O(r^3N)$ operations required to calculate the sums S_{jrp} on the right-hand sides of (3.1*a*, *b*). Input/output times are also significant because of the $O(r^2N)$ data values which need to be stored.

4. The flow quantities of interest

The aim of this paper is to determine whether a singularity develops in the unsteady boundary-layer equations prior to the breakaway of a free shear layer (i.e. separation). Because (i) the outer irrotational flow is significantly changed by separation, and (ii) it is viscous displacement velocity v_∞ at the edge of the boundary layer that drives the perturbation to the outer flow, v_∞ can be expected to grow rapidly as separation is approached. Consequently, v_∞ should be a good indicator of the presence of any singularity.

The boundary-layer displacement thickness δ is another possible indicator of

separation. However, it is a less sensitive guide, as illustrated by the Goldstein singularity for which v_∞ is infinite but δ is bounded. Further, unlike steady flows over fixed walls, it is not necessarily true for unsteady flows that separation is synonymous with the onset of wall shear reversal (Sears & Telionis 1975). Therefore, an examination of the wall shear τ is less likely to reveal details of any singularity. However, in order for comparisons to be made with previous authors' work, graphs of τ and δ, in addition to v_∞, will be presented.

First, the following series representations for τ, δ and v_∞ are deduced from (2.2):

$$\tau(x,t) = u_y(x,0,t) = (4t)^{-\frac{1}{2}} \sum_{r=0}^{\infty} t^r \sum_{p=1}^{r+1} f''_{rp}(0) \sin px, \tag{4.1a}$$

$$\begin{aligned}\delta(x,t) &= \int_0^\infty \left(1 - \frac{u}{\sin x}\right) \mathrm{d}y \\ &= 2t^{\frac{1}{2}} \left(\pi^{-\frac{1}{2}} - \sum_{r=1}^{\infty} t^r \sum_{p=1}^{r+1} f_{rp}(\infty) \frac{\sin px}{\sin x}\right),\end{aligned} \tag{4.1b}$$

$$\begin{aligned}v_\infty(x,t) &= \lim_{y\to\infty} (v + y\cos x) \\ &= 2t^{\frac{1}{2}} \left(\pi^{-\frac{1}{2}} \cos x - \sum_{r=1}^{\infty} t^r \sum_{p=1}^{r+1} f_{rp}(\infty)\, p \cos px\right).\end{aligned} \tag{4.1c}$$

Each of these series is of the form

$$g(x,t) = \sum_{r=0}^{\infty} a_r(x)\, t^r. \tag{4.2a}$$

The convergence of such series in the *complex-time* plane is confined to those times for which $|t| < |t^*(x)|$, where $t^*(x)$ is the location of the nearest singularity to the origin. For times with larger moduli, an approximate method of analytic continuation is provided by Padé approximants, or alternatively continued fractions. Padé approximants have the form

$$P_N^M(x,t) = \frac{\sum_{r=0}^{M} b_r(x)\, t^r}{\sum_{p=0}^{N} d_p(x)\, t^p}, \quad d_0 = 1. \tag{4.2b}$$

Continued fractions are an equivalent representation of the P_N^N and P_{N+1}^N Padé approximants, and have the form

$$c_L(x,t) = c_0(x)/(1 + c_1(x)\, t/(1 + c_2(x)\, t/\ldots/(1 + c_L(x)\, t)\ldots)). \tag{4.2c}$$

The b_r, c_r and d_r are determined uniquely by equating coefficients of equal powers of t between (4.2*a*) and the Taylor-series expansions of (4.2*b*, *c*). In contrast to (4.2*a*), both Padé approximants and continued fractions usually fail to converge only near branch points or branch cuts of g. They are able to represent singularities of g by suitably positioning the poles resulting from the zeros of the polynomial in the denominator. For further details concerning the theory and applications of rational functions see Baker (1965), Graves-Morris (1973), Cabannes (1976) or Bender & Orszag (1978).

Rational functions have been used with success in water-wave theory by Schwartz (1974), Longuet-Higgins (1975), Rottman (1982) and others. Morf, Orszag & Frisch (1980) have also employed Padé approximants in the search for a singularity in the

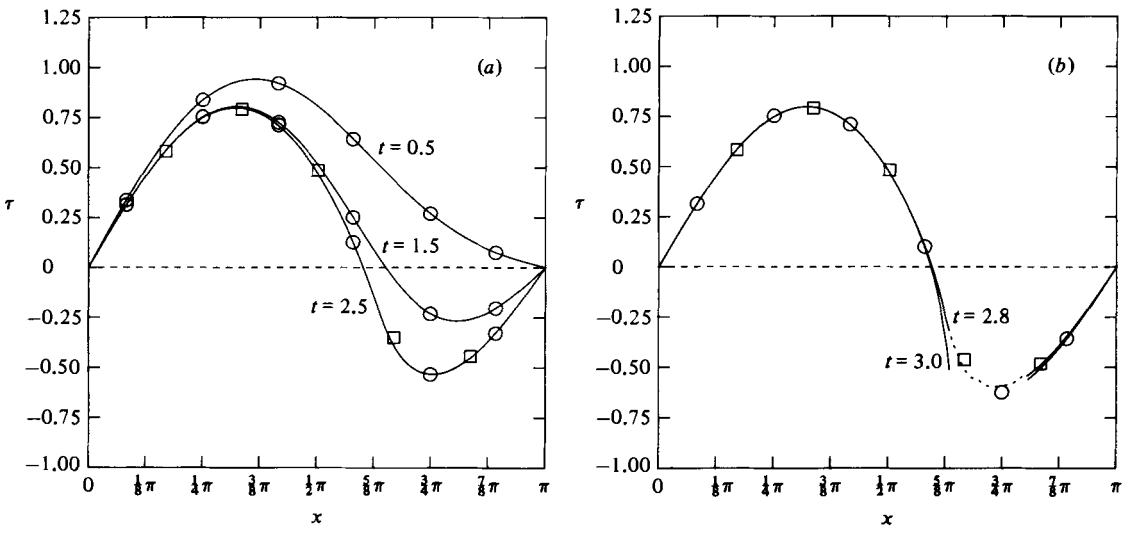

FIGURE 2. Wall shear: ○, van Dommelen & Shen (1980), $t = 0.5, 1.5, 2.5, 3.0$; □, Wang (1982), $t = 2.5, 2.8$.

time evolution of the inviscid Taylor–Green vortex problem. In the present study, as in the Taylor–Green problem, the presence or absence of *poles on the positive time axis* will be of primary importance. However, not all the poles of rational functions represent singularities of the underlying function. Often poles and zeros of rational functions are 'paired', so that in effect they cancel each other out. This is illustrated in figure 7, where the C_{48} continued fraction has a pole/zero pair at $t \approx 1.31$ which is absent in the C_{47} continued fraction. This suggests that the C_{48} pole/zero pair is spurious. Consequently, it is important to determine the positions of both poles and zeros in a search for singularities. The position and time at which a singularity develops is determined by that unpaired pole lying on the real positive time axis which is closest to the origin.

Wall shear

In figure 2 the wall shear has been plotted using the P^{24}_{25} Padé approximant. A continuous curve has been drawn where the differences between successive Padé approximants cannot be distinguished to within graphical accuracy. Between 0.62π and 0.82π insufficient terms of the Padé approximant are known for an accurate curve to be drawn for $t \gtrsim 2.7$. An approximate dashed curve is included for $t = 2.8$, but the spurious poles and zeros present mean that a meaningful curve cannot be drawn for $t = 3.0$. With the exception of positions in the sector $0.62\pi \lesssim x \lesssim 0.82\pi$ when $t \gtrsim 2.7$, the agreement between our solution and those of van Dommelen & Shen (1980) and Wang (1982) is excellent.

Following Blasius (1908), many authors have found the time t_0 when the wall shear first reverses at $x = \pi$, and have plotted the subsequent position of the point of zero wall shear x_z. We find that $t_0 = 0.643\,839\,78$, which compares favourably with the results of Collins & Dennis (1973*b*): 0.644, Cebeci (1979): 0.640, van Dommelen (1981): 0.644 and Hommel (1982): 0.643 839 707. In figure 3 we have plotted the position of zero wall shear using six different continued fractions. The agreement between our results and those of van Dommelen & Shen (1980), in particular, is excellent. The dotted line in figure 3 was plotted using two different truncations of

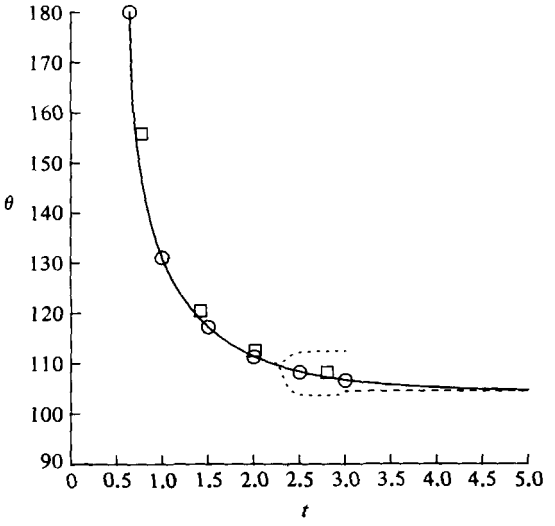

FIGURE 3. Position of point of zero wall shear: —, C_{46}, C_{47}, C_{48}, C_{49}, C_{50} and C_{51} continued-fraction solutions all superimposed; . . ., solutions from Taylor series with 46 and 50 terms; --, position of steady Goldstein singularity found by Terrill (1960); ○, van Dommelen & Shen (1980); □, Wang (1982).

the Taylor series for the wall shear. For $t \gtrsim 2.2$ it is clear that the Taylor series breaks down, and the use of rational functions is necessary.

As $t \to \infty$, the position of zero wall shear appears to be tending to the position of the Goldstein singularity for steady classical boundary-layer flow past a cylinder (Terrill 1960). This is despite the fact that classical boundary-layer theory is known not to describe steady flow past a cylinder (Smith 1979). However, if a singularity develops at some time t_s and position x_s, then it is likely that this singularity will disrupt the outer flow and so invalidate figure 3 for the larger values of t plotted.

Displacement thickness

In figure 4 the displacement thickness has been plotted using the C_{47} continued fraction. For $t \gtrsim 2.5$ a complete curve cannot be drawn because insufficient terms of the continued fraction are known. However, at those values of x for which the displacement function can be calculated there is again excellent agreement with the solution of van Dommelen & Shen (1980). Good agreement is also found with Wang (1982), and on $x = \pi$ with Robins & Howarth (1972), and Hommel (1982). The latter two investigations were concerned with the solution of the similarity equation obtained by Taylor-expanding about the rear stagnation point (Proudman & Johnson 1962).

The rear stagnation-point flow

The flow at the rear stagnation point has previously been calculated using a series-extension technique by Hommel (1982). He solved a system of ordinary differential equations similar to (2.3), and obtained coefficients in the Taylor series for wall shear and displacement thickness, $\bar{f}''_{r+1}(0)$ and $\bar{f}_{r+1}(\infty)$ respectively, which are related to our coefficients by

$$\bar{f}''_{r+1}(0) = (-)^r \sum_{p=1}^{r+1} p f''_{rp}(0), \quad \bar{f}_{r+1}(\infty) = (-)^r \left(\pi^{-\frac{1}{2}} - \sum_{p=1}^{r+1} p f_{rp}(\infty) \right). \quad (4.3a, b)$$

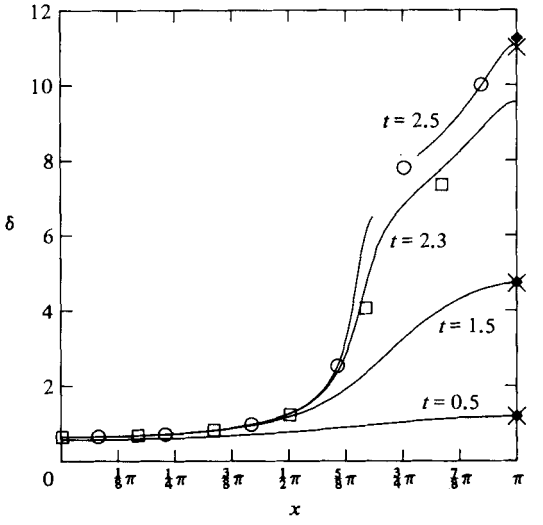

FIGURE 4. Displacement thickness: ○, van Dommelen & Shen (1980), $t = 2.5$; □, Wang (1982), $t = 2.3$; ◆, Robins & Howarth (1972), $t = 0.5, 1.5, 2.5$; ×, Hommel (1982), $t = 0.5, 1.5, 2.5$.

His method of numerical integration is similar to ours. However, he used $\eta_\infty = 5$ or $\eta_\infty = 12.5, \bar{f}'_{r+1}(\eta_\infty) = 0$ and an $O(h^4)$ method, as opposed to our larger values of η_∞, asymptotic outer boundary conditions and $O(h^6)$ method.

A comparison of the two sets of wall-shear coefficients is favourable up to $r \approx 32$. For $r \gtrsim 34$ there is no discernible pattern in the signs of our coefficients, suggesting that we have reached the limit of our accuracy (for a general discussion of the sign patterns of series coefficients see Van Dyke 1980). Hommel (1982) claims accuracy beyond this point, although his sign pattern changes for $r > 52$. Indeed, Hommel's 'direct' expansion method should be more accurate than ours,† because we incur a certain loss of accuracy when summing the coefficients in (4.3*a*, *b*). Furthermore, an examination of the wall-shear coefficients

$$\sum_{p=1}^{r+1} \bar{f}''_{rp}(0) \sin px$$

for other values of x demonstrates that the error generated by cancellation is most severe at $x = \pi$ (e.g. $\bar{f}''_{31}(0) = 1.7 \times 10^{-15}$ while $\max_p \bar{f}''_{30p}(0) = 2.1 \times 10^{-12}$). The less significant cancellation at other angles means that at $x = \frac{5}{6}\pi$, for instance, our wall-shear coefficients have basic sign pattern $+ + - -$ to as many terms as have been calculated.‡

The severe cancellation incurred in summing the wall-shear series (4.3*a*) is absent in summing the series (4.3*b*). Consequently, our displacement-thickness coefficients are found to have the regular sign pattern $+ + + - - -$ to as many terms as have been calculated. Owing to restrictions in his numerical method, Hommel (1982) reports only the first 17 coefficients. It is interesting that he found greater difficulty in calculating $\bar{f}_{r+1}(\infty)$ than $\bar{f}''_{r+1}(0)$, since our calculations suggest that we know the former to more figures than the latter (see §3). The regularity of the sign pattern of

† Hommel's method cannot, however, be extended to $x \neq \pi$.

‡ In fact, this pattern 'skips a beat' at $r = 29$, but this is not unusual (Van Dyke 1980).

t	Hommel $\tau(\pi,t)$	Present $\tau(\pi,t)$	Hommel $\delta(\pi,t)$	Present $\delta(\pi,t)$	Present $\delta_1(\pi,t)$
0.5	0.188418298	0.188418335	1.195974	1.195984526 65	1.195984526 65
1.0	−0.340102048	−0.340101709	2.6026	2.602651663 53	2.602651663 53
1.5	−0.666419214	−0.666417892	4.719	4.720534699 5	4.720534699 5
2.0	−0.884219 20	−0.884215 56	7.5	7.535955 83	7.535955 83
2.5	−1.022 39	−1.022382 7	11.0	11.083 600	11.083 600
3.0	−1.104 79	−1.104 775	15.0	15.808 1	15.808 1
3.5	−1.152 4	−1.152 42	20.0	22.662	22.662
4.0	−1.180	−1.180 4		33.15	33.15
4.5	−1.197	−1.197 6		49.5	49.5
5.0	−1.210	−1.209		75	75

TABLE 1

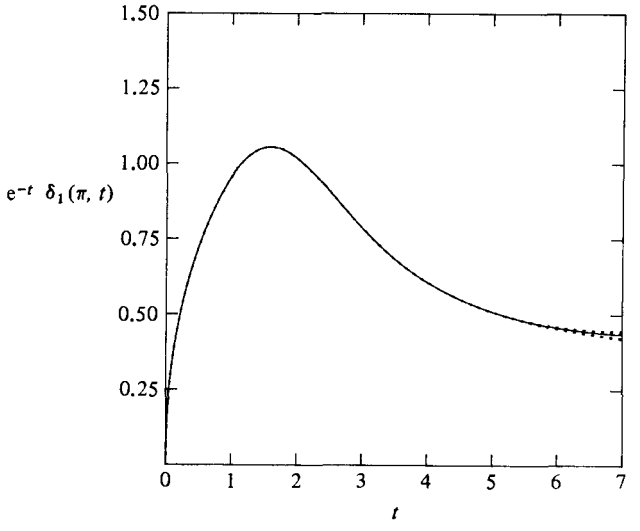

FIGURE 5. Plot of $e^{-t}\delta_1(\pi,t)$: . . . . . , C_{42}, C_{43}, C_{45}, C_{46}, C_{47}, C_{48} continued-faction representations; ——, average of the six continued-fraction solutions.

both the wall-shear coefficients and the displacement-thickness coefficients gives us confidence in our results.

A comparison of the wall shear and displacement thickness calculated using our coefficients and Hommel's is given in table 1. Our results were checked using different runs and different-order continued fractions, and are believed to be correct to as many figures as are given. The small differences that exist are possibly a result of our more accurate numerical method.

In addition to calculating the displacement thickness by directly recasting the simple series using rational functions, we have also calculated $\delta(\pi,t)$ by a method suggested by Hommel (1982). In this method, which is based on Proudman & Johnson's (1962) conclusion that $\delta(\pi,t)$ grows like e^t as $t\to\infty$, the series for e^t is first extracted from (4.1*b*) before the continued fraction is formed. Multiplication of this continued fraction by the factor e^t results in the values of the displacement thickness $\delta_1(\pi,t)$ given in table 1. We note that there is good agreement with $\delta(\pi,t)$. In figure 5 we have also plotted $e^{-t}\delta_1(\pi,t)$. The dotted lines are the C_{48}, C_{47}, C_{46}, C_{45}, C_{43} and

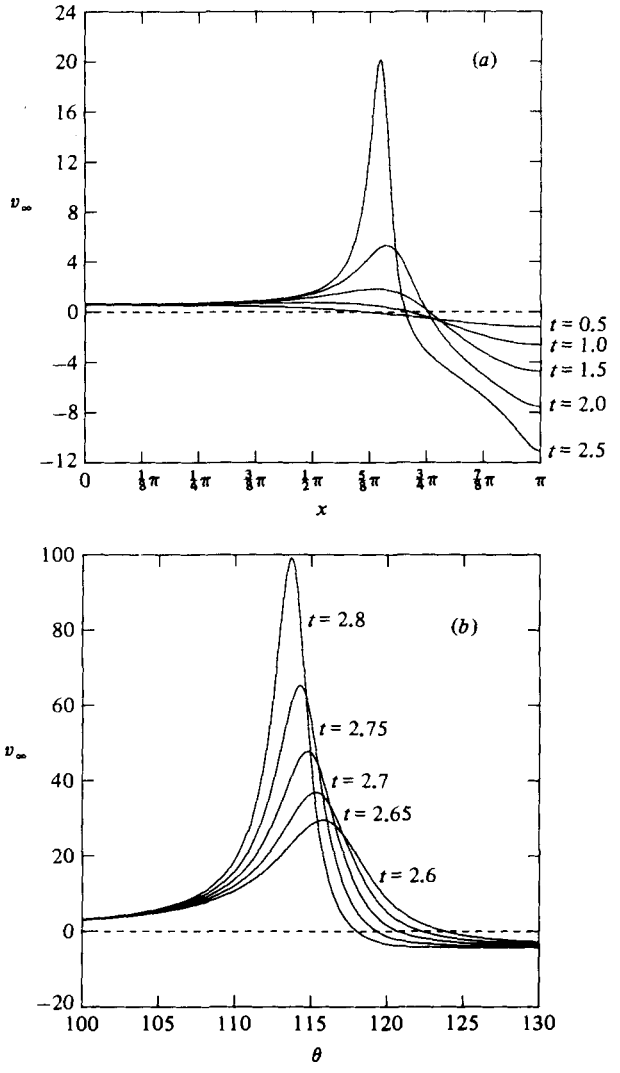

FIGURE 6. Viscous displacement velocity v_∞.

C_{42} continued fractions. The solid line is the average of these. Our results are in reasonable agreement with the prediction that $e^{-t}\,\delta_1(\pi, t)$ tends to a constant as $t \to \infty$.

Viscous displacement velocity

The viscous displacement velocity v_∞ has been plotted in figure 6. Except for angles close to $\theta = 124°$, the graphs were plotted using the C_{50} continued fraction. For $\theta \approx 124°$ the C_{44} continued fraction was used owing to the presence of a spurious pole/zero pair in the C_{50} fraction. Figure 6 (*a*) is correct to at least graphical accuracy, but the curves for large times in figure 6 (*b*) could be up to 10 % out. The C_{50} and C_{44} continued fractions were used because for $t = 2.8$ they were the only continued fractions that were not disrupted close to the maximum of v_∞ by spurious poles and zeros. The rapid growth in the peak of v_∞ suggests the development of a singularity.

Previous authors have not tabulated v_∞ because it can only be obtained indirectly

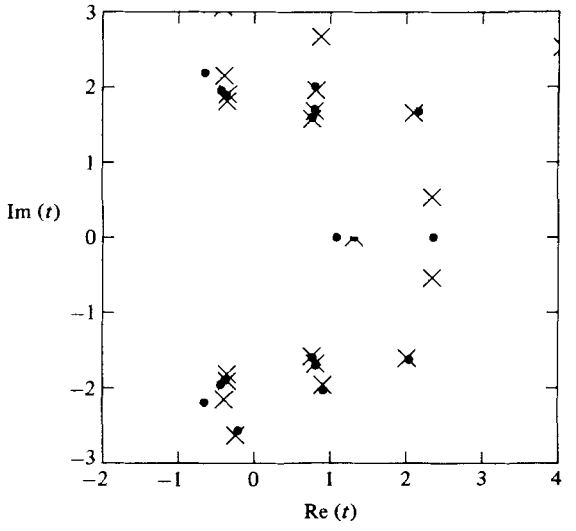

FIGURE 7. Positions of the poles and zeros of v_∞ in the complex-time plane for $\theta = 130°$: ●, zero; ×, pole. $\mathrm{Im}(t) = 0$ drawn using C_{47}, $\mathrm{Im}\,(t) < 0$ drawn using C_{48}.

from their results (e.g. by the numerical differentiation of $\delta(x, t) \sin x$ by x). However, it is interesting that the present series method is complementary to other methods in that it finds v_∞ to greater accuracy than δ and τ, whereas for previous Eulerian and Lagrangian methods it was *vice versa*.

5. The singularity in v_∞

If a singularity develops in v_∞, this should be evident by examining the poles and zeros of the rational functions in the complex-time plane at various values of θ. In figure 7 the positions of the poles and zeros closest to the origin have been plotted for a typical angle in the range of interest ($\theta = 130°$). The poles and zeros of the C_{47} and C_{48} continued fractions are given in the top and bottom halves of the figure respectively. Because the coefficients of the series are real, $\mathrm{Im}\,(t) > 0$ should be the complex conjugate of $\mathrm{Im}\,(t) < 0$. We note that, in the vicinity of the origin, the positioning of the poles and zeros by the two different continued fractions is consistent, except for the pole/zero pair at $t \approx 1.31$ for C_{48} which has been discussed above. Farther from the origin, not enough terms of the continued fraction are known to specify the positions of the poles and zeros precisely. The two zeros on the real positive axis and the complex-conjugate pair of poles at $t = (2.35, \pm 0.54\mathrm{i})$ turn out to be of most relevance. As demonstrated below, these poles move toward and then hit the real positive time axis as θ varies, so confirming the presence of a singularity in the boundary-layer equations.

In figure 8 the motion of these two poles and the neighbouring two zeros is plotted as θ varies. We see that

(i) for $\theta = 75°$ there is one zero on the negative real axis;

(ii) as θ increases through 90° the zero moves through onto the positive real axis;

(iii) for $\theta \gtrsim 104°$ a pole appears on the positive real axis at large values of t;

(iv) as θ increases further the pole and zero move towards each other, until, for $\theta \approx 111°$, the pole splits into a complex-conjugate pair of poles together with a zero on the real axis;

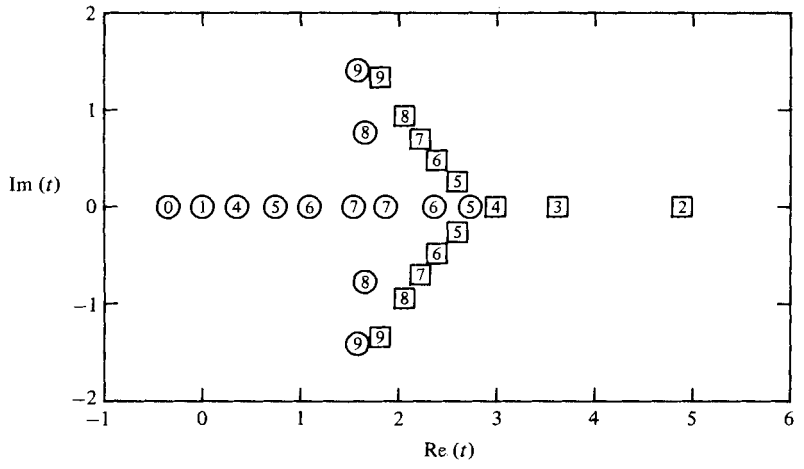

FIGURE 8. Movement of poles (□) and zeros (○) of v_∞ as θ varies: 0, 75°; 1, 90°; 2, 105°; 3, 107°; 4, 111°; 5, 120°; 6, 130°; 7, 136°; 8, 145°; 9, 160°.

(v) for larger values of θ the zeros move towards each other, hit when $\theta \approx 136°$, and then move off the real axis as a complex-conjugate pair of zeros.

The prediction of a pole on the real axis confirms the proposals of van Dommelen & Shen (1980) and others that a singularity develops in the classical boundary-layer equations at a finite time t_s. The value of t_s and the position θ_s at which the singularity develops are determined by the position where the single pole splits into two complex-conjugate poles and a zero. We do not have enough terms in our continued fractions to determine this precisely. This is because, when two poles and a zero are close together, a finite continued fraction tends to approximate them by a single pole.

In figure 9 we have plotted the coordinates of the poles and zero for those angles for which the different-order continued fractions available give a consistent result. The portion of the curve plotted for the imaginary coordinate of the pole appears approximately linear, but this does not guarantee that the curve will remain linear down to Im $(t) = 0$ (see below). A linear extrapolate predicts that the pole intersects the real time axis at $\theta_s \approx 111\frac{1}{2}°$. From the coordinate of the single pole on the real time axis, it then follows that $t_s \approx 3.0$. These results are consistent with those given by van Dommelen (1981): $\theta_s \approx 111.0°$, $t_s \approx 3.00$.

An analytic structure for the boundary-layer singularity has been proposed by van Dommelen & Shen (1982). Using a Lagrangian approach they deduced that, for $t_s - t \ll 1$,

$$\delta \sim (t_s - t)^{-\frac{1}{4}} \int_{U_0}^{\infty} \frac{\lambda \, \mathrm{d}U}{[U^3 + \Phi_0(U + \gamma X)]^{\frac{1}{2}}}, \tag{5.1a}$$

where

$$x - x_s \sim -U_s(t_s - t) + X(t_s - t)^{\frac{3}{2}}, \tag{5.1b}$$

$$U_0^3 + \Phi_0(U_0 + \gamma X) = 0, \quad \Phi_0 > 0. \tag{5.1c}$$

λ, γ, Φ_0 and U_s are constants. The form of this singularity has been confirmed by Elliott, Cowley & Smith (1983) by means of an Eulerian approach. From (5.1) it follows that

$$v_\infty \sim 6\lambda\Phi_0 \sin x_s (t_s - t)^{-\frac{7}{4}} \int_{U_0}^{\infty} \frac{U \, \mathrm{d}U}{(3U^2 + \Phi_0)^2 (U^3 + \Phi_0(U + \gamma X))^{\frac{1}{2}}}. \tag{5.2}$$

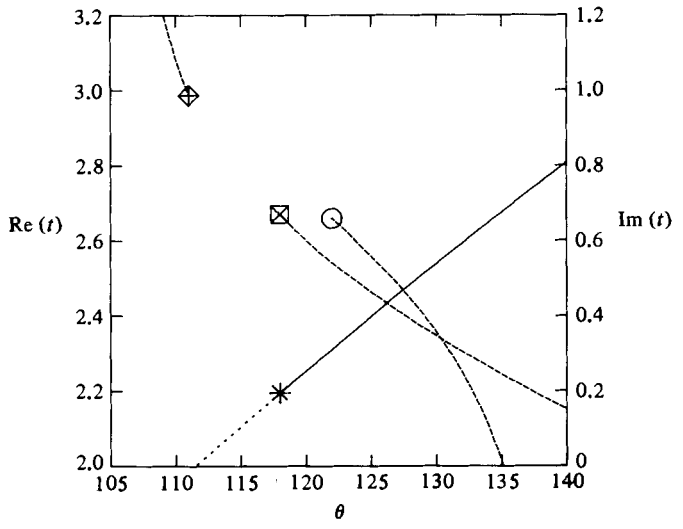

FIGURE 9. Coordinates of zero and poles in the complex-time plane. Left ordinate is real part of t; right ordinate is imaginary part of t. ⊖––, real coordinate of zero ($\theta > \theta_s$). ⊕––, real coordinate of pole ($\theta < \theta_s$); ⊠––, real coordinate of poles ($\theta > \theta_s$); ✳—, imaginary coordinate of pole in upper half-plane ($\theta > \theta_s$); . . . . . , linear extrapolate of imaginary coordinate.

It can be shown that the integral in (5.2) is a meromorphic function with (i) a complex-conjugate pair of poles at $X = \pm iX_p \equiv \pm i(4\Phi_0/27\gamma^2)^{\frac{1}{2}}$ and (ii) a zero at X_z on the real X-axis. In the complex-time plane, the position of the zero of v_∞ is given by

$$t_s - t = \left(\frac{x_s - x}{U_s}\right) + \left(\frac{x_s - x}{U_s}\right)^{\frac{3}{2}} \frac{X_z}{U_s} + \ldots, \tag{5.3a}$$

while the positions of the poles are given by

$$\mathrm{Re}\,(t_s - t) = \left(\frac{x_s - x}{U_s}\right) + \ldots, \tag{5.3b}$$

$$\mathrm{Im}\,(t_s - t) = \pm\left(\frac{x_s - x}{U_s}\right)^{\frac{3}{2}} \frac{X_p}{U_s} + \ldots. \tag{5.3c}$$

The prediction of (5.2) that for $x > x_s$ the local solution for v_∞ near t_s should include two simple poles and a zero is in agreement with our results using continued fractions (see figure 8). However, the agreement between (5.3) and figure 9 is less satisfactory. In particular, the slope of the curve for the imaginary coordinate of the pole should decrease to zero as x_s is approached. In contrast, the curves for the real coordinates of the poles and zero should be tending to straight lines with the same slope. The reason for this mismatch is probably that insufficient terms of the series have been calculated. We also conclude that the linear extrapolation of $\mathrm{Im}\,(t_s - t)$ used above to find θ_s probably yields an overestimate of θ_s (compare our prediction of $111\frac{1}{2}°$ and the 111.0° of van Dommelen 1981).

Another possible check of (5.2) is on the maximum value of v_∞. This should grow like $(t_s - t)^{-\frac{7}{4}}$. Figure 10 is a logarithmic plot of $\max_\infty(v_\infty)$ against $t_s - t$ obtained using the 50-term continued fraction and van Dommelen's value of $t_s = 3.00$. Also plotted is a straight line with slope $\frac{7}{4}$. The slopes of the two curves are in good agreement.

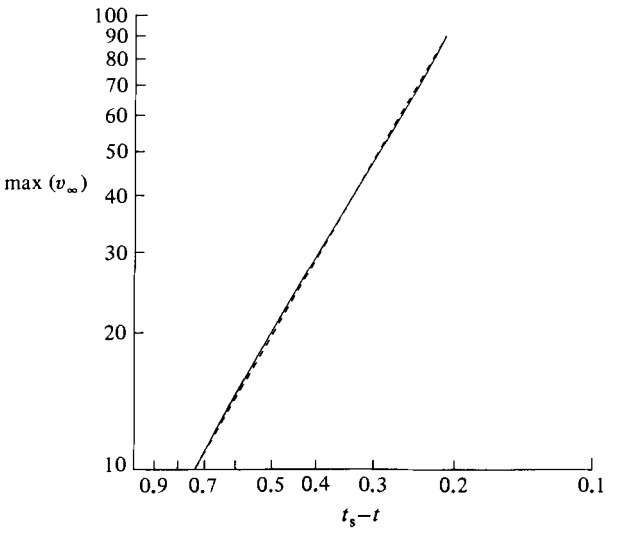

FIGURE 10. Logarithmic plot of max (v_∞) against (t_s-t).

6. Conclusions

The classical unsteady boundary-layer equations describing impulsive flow past a circular cylinder have been studied by extending Blasius' (1908) series solution to 51 terms. The resulting 676 ordinary differential equations governing the flow have been solved using an accurate finite-difference scheme. In order to extend the validity of the solution, Blasius' simple series expansion is recast using rational functions.

For $t \lesssim 2.5$ good agreement for the wall shear and displacement thickness is obtained between the present work and that of previous authors. For larger times, the presence of spurious poles and zeros in the rational functions leads to the breakdown of our solution for $110° \lesssim \theta \lesssim 145°$. This range of θ would be decreased if more terms of the series were available. In the case of the viscous displacement velocity, our solution remains valid to slightly larger times.

An analysis of the poles and zeros of the rational function approximations for v_∞ suggests that for $105° \lesssim \theta \lesssim 111°$ there is a simple pole on the positive real time axis. This pole is closest to the time origin for $\theta = \theta_s \approx 111°$, which suggests that a singularity will develop in the boundary-layer equations at θ_s when $t = t_s \approx 3.0$. An examination of the solution of the boundary-layer equations *for all* x therefore predicts the breakdown of this solution at a finite time. In contrast, Proudman & Johnson's (1962) similarity solution for the flow at a rear stagnation point exhibits breakdown only as $t \to \infty$.

For $\theta > \theta_s$, the present solution for v_∞ predicts that there will be two poles and a zero in the neighbourhood of the complex-time plane surrounding t_s. In turn, this suggests that $\max_x(v_\infty)$ should grow like $(t_s-t)^{-q}$, where $1 < q < 2$. Both these predictions are in agreement with the asymptotic structure proposed for this unsteady singularity by van Dommelen & Shen (1982). Further, our results are consistent with their proposal that $q = \frac{7}{4}$.

As a result of the development of a singularity, the outer flow will be disturbed for $t \gtrsim t_s$ (Elliott *et al.* 1983). Consequently, the present solution may have no relevance for $t \gtrsim t_s$ for *any* x. *If* the outer flow were not changed significantly, the present solution would predict that as t increases from t_s the singularity would move towards the

forward face of the cylinder. In particular, it suggests that as $t \to \infty$ the position of the singularity would tend to θ_G where $104° < \theta_G < 105°$. This result is consistent with the eventual formation of a steady Goldstein singularity at $\theta = 104.5°$, as predicted by Terrill's (1960) solution for steady classical boundary-layer flow past a cylinder.

With hindsight, we see that it would have been possible to search for the presence of singularities in the boundary-layer equations by using the displacement thickness instead of v_∞. For it follows from (5.1*a*) that there are logarithmic singularities in δ at $X = \pm iX_p$. However, while rational functions can represent poles exactly, branch points and branch cuts can only be approximated by placing alternate zeros and poles along the branch cut. Consequently, rational functions should be able to represent v_∞ more accurately than δ. This may explain why the present representations of v_∞ remain valid to larger times than those for δ (compare figures 4 and 6). Certainly, it should be easier to identify a singularity using v_∞ rather than δ.

The reason why the rational functions have difficulty representing the wall shear is less easily understood, for the wall shear remains regular at t_s (van Dommelen & Shen 1982). A tentative explanation might be that the explosive exodus of fluid out of the boundary layer for $t > t_s$ might draw fluid towards θ_s, so causing the re-reversal of wall shear (the original point of zero wall shear is at $\theta_z < \theta_s$). The formation of such a *small* counter-rotating eddy, which is supported by the experiments of Bouard & Coutanceau (1980), would be hard for the rational functions to imitate, so leading to the spurious poles and zeros. A check of this hypothesis could in principle be made because van Dommelen & Shen's (1980) Lagrangian method allows integration past t_s. However, the disadvantage of a Lagrangian scheme is that the fluid particles move downstream. To correct for this, the grid points need to be clustered upstream at the start of the calculation. If van Dommelen & Shen's (1980) rectangular grid were to be used, the mesh spacing on the wall near θ_s might not be fine enough to detect the formation of a small eddy for $t > t_s$. Nevertheless, their Lagrangian scheme does appear optimal for $t \approx t_s$. A possible alternative hybrid scheme might therefore be to use a series-extension technique or Eulerian scheme up to $t = 2.0$, say, and then the Lagrangian scheme, but with a less stretched grid, from then on.

Dr T. J. Pedley and Dr F. T. Smith are thanked for useful discussions. The continued-fraction subroutines were kindly supplied by Dr A. J. Roberts and Dr J. W. Rottman.

A preliminary version of this work was presented at EUROMECH 148, 13–15 October 1981, Ruhr-University, Bochum.

REFERENCES

Baker, G. A. 1965 The theory and application of the Padé approximant method. In *Advances in Theoretical Physics* (ed. K. A. Brueckner), vol. 1, pp. 1–58. Academic.

Bar-Lev, M. & Yang, H. T. 1975 Initial flow field over an impulsively started circular cylinder. *J. Fluid Mech.* **72**, 625–647.

Batchelor, G. K. 1967 *An Introduction to Fluid Dynamics.* Cambridge University Press.

Bender, C. M. & Orszag, S. A. 1978 *Advanced Mathematical Methods for Scientists and Engineers.* McGraw-Hill.

Blasius, H. 1908 Grenzschichten in Flüssigkeiten mit kleiner Reibung. *Z. Math. Phys.* **56**, 1–37.

Bouard, R. & Coutanceau, M. 1980 The early stage of development of the wake behind an impulsively started cylinder for $40 < Re < 10^4$. *J. Fluid Mech.* **101**, 583–607.

CABANNES, H. (ed.) 1976 *Padé Approximants Method and its Application to Mechanics.* Lecture Notes in Physics, vol. 47. Springer.

CEBECI, T. 1979 The laminar boundary layer on a circular cylinder started impulsively from rest. *J. Comp. Phys.* **31**, 153–172.

CEBECI, T. 1982 Unsteady separation. In *Numerical and Physical Aspects of Aerodynamic Flows* (ed. T. Cebeci). Springer.

COLLINS, W. M. & DENNIS, S. C. R. 1973*a* Flow past an impulsively started cylinder. *J. Fluid Mech.* **60**, 105–127.

COLLINS, W. M. & DENNIS, S. C. R. 1973*b* The initial flow past an impulsively started circular cylinder. *Q. J. Mech. Appl. Maths* **26**, 53–75.

DENNIS, S. C. R. & STANIFORTH, A. N. 1971 In *Proc. 2nd Intl Conf. on Numerical Methods in Fluid Dynamics.* Lecture Notes in Physics, vol. 8, p. 343. Springer.

ELLIOTT, J. W., COWLEY, S. J. & SMITH, F. T. 1983 Breakdown of boundary layers: (i) on moving surfaces; (ii) in semi-similar unsteady flow; (iii) in fully unsteady flow. *Geophys. Astrophys. Fluid Dyn.* **25**, 77–138.

FOX, L. 1957 *The Numerical Solution of Two-point Boundary Problems in Ordinary Differential Equations.* Clarendon.

GOLDSTEIN, S. & ROSENHEAD, L. N. 1936 Boundary layer growth. *Proc. Camb. Phil. Soc.* **32**, 392–401.

GRAVES-MORRIS, P. R. 1973 *Padé Approximants and their Applications.* Academic.

HOMMEL, M. J. 1982 Ph.D. dissertation, Stanford University. [See also *J. Fluid Mech.* **132** (1983), 407–416.]

INGHAM, D. B. 1983 Unsteady separation. *J. Comp. Phys.* (to appear).

LONGUET-HIGGINS, M. S. 1975 Integral properties of periodic gravity waves of finite amplitude. *Proc. R. Soc. Lond.* A **342**, 157–174.

MORF, R. H., ORSZAG, S. A. & FRISCH, U. 1980 Spontaneous singularity in three-dimensional, inviscid, incompressible flow. *Phys. Rev. Lett.* **44**, 572–575.

NAGATA, H., MINAMI, K. & MURATA, Y. 1979 Initial flow past an impulsively started circular cylinder. *Bull. JSME* **22**, 512–520.

PATEL, V. A. 1976 Time dependent solutions of the viscous incompressible flow past a circular cylinder by the method of series truncation. *Comp. & Fluids* **4**, 13.

PROUDMAN, I. & JOHNSON, K. 1962 Boundary-layer growth near a rear stagnation point. *J. Fluid Mech.* **12**, 161–168.

ROBINS, A. J. & HOWARTH, J. A. 1972 Boundary-layer development at a two-dimensional rear stagnation point. *J. Fluid Mech.* **56**, 161–171.

ROTTMAN, J. W. 1982 Steep standing waves at a fluid interface. *J. Fluid Mech.* **124**, 283–306.

SCHWARTZ, L. W. 1974 Computer extension and analytic continuation of Stokes' expansion for gravity waves. *J. Fluid Mech.* **62**, 553–578.

SCHLICHTING, H. 1968 *Boundary-Layer Theory*, 6th edn. McGraw-Hill.

SEARS, W. R. & TELIONIS, D. P. 1975 Boundary-layer separation in unsteady flow. *SIAM J. Appl. Maths* **28**, 215–235.

SMITH, F. T. 1979 Laminar flow of an incompressible fluid past a bluff body: the separation, reattachment, eddy properties and drag. *J. Fluid Mech.* **92**, 171–205.

SON, J. S. & HANRATTY, T. J. 1969 Numerical solution for the flow around a cylinder at Reynolds numbers of 40, 200 and 500. *J. Fluid Mech.* **35**, 369–386.

TA PHUOC LOC 1980 Numerical analysis of unsteady secondary vortices generated by an impulsively started circular cylinder. *J. Fluid Mech.* **100**, 111–128.

TERRILL, R. M. 1960 Laminar boundary-layer flow near separation with and without suction. *Phil. Trans. R. Soc. Lond.* A **253**, 55–100.

THOMAN, D. C. & SZEWCZYK, A. A. 1969 Time-dependent viscous flow over a circular cylinder. *Phys. Fluids Suppl.* **12**, II, 78–86.

VAN DOMMELEN, L. L. 1981 Unsteady boundary layer separation. Ph.D. dissertation, Cornell University.

VAN DOMMELEN, L. L. & SHEN, S. F. 1980 The spontaneous generation of the singularity in a separating laminar boundary layer. *J. Comp. Phys.* **38**, 125–140.

VAN DOMMELEN, L. L. & SHEN, S. F. 1982 The genesis of separation. In *Numerical and Physical Aspects of Aerodynamic Flows* (ed. T. Cebeci). Springer.

VAN DYKE, M. 1980 Notes on computer-extended series in mechanics. *20th Summer Research Institute of the Australian Mathematical Society.*

WANG, C.-Y. 1967 The flow past a circular cylinder which is started impulsively from rest. *J. Maths & Phys.* **46**, 195–202.

WANG, K. C. 1979 Unsteady boundary layer separation. *Martin Marietta Lab., Baltimore, Maryland, USA, Tech. Rep.* MML TR 79-16C.

WANG, K. C. 1982 On the current controversy about unsteady separation. In *Numerical and Physical Aspects of Aerodynamic Flows* (ed. T. Cebeci). Springer.

WUNDT, H. 1955 Wachstum der laminaren Grenzchicht an schräg angeströmten Zylindren bei Anfahrt aus der Ruhe. *Ing.-Arch.* **23**, 212–230.